Current Applied Physics 19 (2019) 55–59

Contents lists available at ScienceDirect

Current Applied Physics

journal homepage: www.elsevier.com/locate/cap

Pressure effects on EXAFS Debye-Waller factor and melting curve of solid krypton

Khac Hieu Ho[a,*], Viet Tuyen Nguyen[b], Nguyen Van Nghia[c], Nguyen Ba Duc[d], Vu Quang Tho[d], Tran Thi Hai[e], Doan Quoc Khoa[f,g,**]

[a] Institute of Research and Development, Duy Tan University, 03 Quang Trung, Danang, Viet Nam
[b] VNU University of Science, 334 Nguyen Trai, Thanh Xuan, Hanoi, Viet Nam
[c] Faculty of Energy, Thuyloi University, 175 Tay Son, Dong Da, Hanoi, Viet Nam
[d] Tan Trao University, Tuyen Quang, Viet Nam
[e] Hong Duc University, Thanh Hoa, Viet Nam
[f] Division of Computational Physics, Institute for Computational Science, Ton Duc Thang University, Ho Chi Minh City, Viet Nam
[g] Faculty of Electrical and Electronics Engineering, Ton Duc Thang University, Ho Chi Minh City, Viet Nam

ARTICLE INFO

Keywords:
EXAFS
Debye-Waller factor
Melting curves
High pressure
Statistical moment method

ABSTRACT

The pressure effects on atomic mean-square displacement, extended X-ray absorption fine structure (EXAFS) Debye-Waller factor and melting temperature of solid krypton have been investigated in within the statistical moment method scheme in quantum statistical mechanics. By assuming the interaction between atoms can be described by Buckingham potential, we performed the numerical calculations for krypton up to pressure 120 GPa. Our calculations show that the atomic mean-square displacement and EXAFS Debye-Waller factor of krypton crystal depend strongly on pressure. They make the robust reduction of the EXAFS peak height. Our results are in good and reasonable agreements with available experimental data. This approach gives us a relatively simple method for qualitatively calculating high-pressure thermo-physical properties of materials. Moreover, it can be used to verify future high-pressure experimental and theoretical works.

1. Introduction

In recent years, high-pressure physics is motivated by the remarkable developments of experimental techniques. Researchers could utilize various methods to investigate the thermo-mechanical properties of materials at high pressures (up to hundreds of gigapascals) [1–3]. Rare gases are among the most widely interested materials, both experimentally and theoretically. Firstly, because of their relatively simple system with closed-shell electronic configuration, they are the best candidates for model verification. Secondly, the high-pressure thermodynamic properties of rare gases are of important information for geophysical research (e.g, the unexpectedly low absolute abundance of xenon observed in the atmospheres of both Earth and Mars, especially, the composition, structure and formation of Earth as well as planetary) [4]. Furthermore, rare gases have been extensively used as a pressure medium in high-pressure diamond anvil cell (DAC) experiments. Recently, the properties of solid krypton has been measured to very high pressure by *in situ* X-ray diffraction (XRD) and extended X-ray absorption spectroscopy, about 140 GPa [5]. Therefore, building a theory to determine the thermodynamic properties of solid rare gases under high pressure is the inspiring subject in physics.

Many previous X-ray diffraction studies suggested that solid krypton crystallizes in the face-centered cubic (FCC) structure and it is predicted to remain stable in FCC structure up to pressure 110 GPa [6]. On the theoretical side, the first-principles total energy calculations figured out the FCC-to-hexagonal close-packed (HCP) transition in Kr occurring above 130 GPa [7]. Its equation-of-state (EOS) *PVT* relationship has been derived by many authors with different approaches such as X-ray absorption spectroscopy measurements up to 140 GPa [5,8,9] and energy-dispersive X-ray techniques up to 55 GPa [4,10–12]. Along with the X-ray absorption spectroscopy measurements, the pressure effects on the extended X-ray absorption fine structure spectroscopy (EXAFS) Debye-Waller factor of Kr have been investigated experimentally as well as theoretically up to pressure about 30 GPa [8,9]. And moreover, the pressure-dependent melting curve of Kr crystal has been derived by several authors up to 120 GPa [4,13,14].

* Corresponding author.
** Corresponding author.
E-mail addresses: hieuhk@duytan.edu.vn (K.H. Ho), doanquockhoa@tdtu.edu.vn (D. Quoc Khoa).

https://doi.org/10.1016/j.cap.2018.11.005
Received 26 September 2018; Received in revised form 2 November 2018; Accepted 6 November 2018
Available online 13 November 2018

In this work, based on the statistical moment method (SMM) in quantum statistical mechanics [15,16], we investigate the pressure effects on the EXAFS Debye-Waller factor and melting curve of solid krypton. The pressure-dependent atomic mean-square displacement (MSD) $\langle u^2\rangle$ and SMM EOS have also been considered. Numerical calculations will be performed for a wide pressure range. We compared all of our determinations with recent experimental and theoretical studies as applicable.

2. Theory

2.1. Brief report of statistical moment method

In the first part of the paper, we summarized some main formula of thermodynamic properties which had been derived for crystalline materials in within of the SMM scheme. Let us assume the interatomic potential between two intermediate atoms could be described by $\varphi_{ij}(r)$ function. By expanding the potential energy $\varphi_{i0}(|r_i + u_i|)$ up to fourth-order of the atomic displacement u_i, the author derived the force balance relation as the differential equation of the first-order moment $y \equiv \langle u_i\rangle_p$ [17].

$$\gamma\theta^2\frac{d^2y}{dp^2} + 3\gamma\theta y\frac{dy}{dp} + ky + \gamma\frac{\theta}{k}(X-1) - p = 0, \tag{1}$$

where $\theta = k_BT$ (k_B is the Boltzmann constant, T is the absolute temperature), $x = \hbar\omega/2\theta$, $X = x\coth x$, p is a supplementary force acting on the zeroth central atom in the lattice due to the thermal lattice vibration effects; and harmonic k and anharmonic γ parameters are defined as the following

$$k = \frac{1}{2}\sum_i\left(\frac{\partial^2\varphi_{i0}}{\partial u_{ix}^2}\right)_{eq} \equiv m\omega^2, \tag{2a}$$

$$\gamma = \frac{1}{12}\left\{\sum_i\left[\left(\frac{\partial^4\varphi_{i0}}{\partial u_{ix}^4}\right)_{eq} + 6\left(\frac{\partial^4\varphi_{i0}}{\partial u_{ix}^2\partial u_{iy}^2}\right)_{eq}\right]\right\}. \tag{2b}$$

The solution of differential equation (1) gives us the average atomic displacement $y(T)$ which takes into account the anharmonicity effects of thermal lattice vibrations at temperature T as [15,18].

$$y(T) \approx y_0(T) + A_1p + A_2p^2, \tag{3}$$

where

$$y_0(T) \approx \sqrt{\frac{2\gamma\theta^2}{3k^3}A}, \tag{4}$$

$$A = a_1 + \frac{\gamma^2\theta^2}{k^4}a_2 + \frac{\gamma^3\theta^3}{k^6}a_3 + \frac{\gamma^4\theta^4}{k^8}a_4 + \frac{\gamma^5\theta^5}{k^{10}}a_5 + \frac{\gamma^6\theta^6}{k^{12}}a_6, \tag{5}$$

$$A_1 = \frac{1}{k}\left[1 + \frac{2\gamma^2\theta^2}{k^4}\left(1+\frac{X}{2}\right)(X+1)\right], \tag{6}$$

$$A_2 \approx \frac{1}{2ky_0}\left[\frac{1}{3k}(1-X) - \frac{1}{k} - \frac{y_0^2}{\theta}\right], \tag{7}$$

here a_1, a_2, a_3, a_4, a_5, and a_6 are temperature-dependent parameters which were correspondingly defined as [15].

$$\begin{aligned}
a_1 &= 1 + \tfrac{X}{2},\\
a_2 &= \tfrac{13}{3} + \tfrac{47}{6}X + \tfrac{23}{6}X^2 + \tfrac{1}{2}X^3,\\
a_3 &= -\left(\tfrac{25}{3} + \tfrac{121}{6}X + \tfrac{50}{3}X^2 + \tfrac{16}{3}X^3 + \tfrac{1}{2}X^4\right),\\
a_4 &= \tfrac{43}{3} + \tfrac{93}{2}X + \tfrac{169}{3}X^2 + \tfrac{83}{3}X^3 + \tfrac{22}{3}X^4 + \tfrac{1}{2}X^5,\\
a_5 &= -\left(\tfrac{103}{3} + \tfrac{749}{6}X + \tfrac{363}{2}X^2 + \tfrac{391}{3}X^3 + \tfrac{148}{3}X^4 + \tfrac{53}{6}X^5 + \tfrac{1}{2}X^6\right),\\
a_6 &= 65 + \tfrac{561}{2}X + \tfrac{1489}{3}X^2 + \tfrac{927}{2}X^3 + \tfrac{733}{3}X^4 + \tfrac{145}{2}X^5 + \tfrac{31}{3}X^6 + \tfrac{1}{2}X^7.
\end{aligned} \tag{8}$$

The average nearest-neighbor distance (NND) between two intermediate atoms at temperature T can be calculated as the following

$$r(T) = r(0) + y_0(T), \tag{9}$$

where $r(0)$ is the value of NND r at zero temperature. The value of $r(0)$ can be determined from the minimum condition of the potential energy of crystal or by solving the SMM EOS that will be presented in the next subsection 2.3.

2.2. EXAFS Debye-Waller factor of krypton

In structural research, one of the most effective methods for investigation the structure and thermodynamic properties of crystals is EXAFS [19]. The anharmonic EXAFS provides information on structure and thermodynamic parameters of substances and usually has been analyzed by means of cumulant expansion approach [19,20]. The EXAFS oscillation function contains the second cumulant $\sigma^{(2)} = \sigma^2$ which is an important factor in EXAFS analysis since the thermal lattice vibrations influence sensitively the EXAFS amplitudes through the Debye-Waller factor $\exp(-2\sigma^2k^2)$. The second cumulant corresponds to the parallel mean square relative displacement (MSRD) or EXAFS Debye-Waller factor, which is defined as:

$$\sigma^2 = \langle[\vec{R}.(\vec{u_i} - \vec{u_0})]^2\rangle = \langle u_i^2\rangle + \langle u_0^2\rangle - 2\langle u_iu_0\rangle. \tag{10}$$

Here, u_0 and u_i are the atomic displacements of the *zero*th and the *i*th sites from their equilibrium positions; $\vec{R}$ is the unit vector at the *zero*th site pointing towards the *i*th site, and the brackets denote the thermal average. The first two terms on the right-hand side of Eq. (10) are the uncorrelated MSD, while the third term is the parallel displacement correlation function.

In SMM theory, the relation between the first and the second order moment of atomic displacements is described as [18].

$$\langle u_{i\alpha}u_{i\gamma}\rangle_p = \langle u_{i\alpha}\rangle_p\langle u_{i\gamma}\rangle_p + \theta\frac{\partial\langle u_{i\alpha}\rangle_p}{\partial a_\gamma} + \frac{\hbar\delta_{\alpha\gamma}}{2m\omega}\coth\left(\frac{\hbar\omega}{2\theta}\right) - \frac{\theta\delta_{\alpha\gamma}}{m\omega^2}. \tag{11}$$

where $\alpha, \gamma = x, y, z$.

Then the atomic MSD function can be easily derived as follows

$$\langle u_i^2\rangle = \langle u_i\rangle^2 + \theta A_1 + \frac{\theta}{k}(X-1). \tag{12}$$

For crystals that have a basic cubic structure, such as FCC, any directional dependence of $\langle u^2\rangle$ must have cubic symmetry. Hence, in this sense we have approximations as

$$\langle u_j^2\rangle \approx \langle u_0^2\rangle \quad ; \quad \langle u_ju_0\rangle \approx \langle u_j\rangle\langle u_0\rangle. \tag{13}$$

Then we derive the expression of parallel MSRD or EXAFS Debye-Waller factor of cubic crystal as the following

$$\sigma^2(T) \approx \frac{4\gamma^2\theta^3}{k^5}\left(1+\frac{X}{2}\right)(X+1) + \frac{2\theta}{k}X. \tag{14}$$

2.3. High-pressure thermodynamic quantities

In order to consider the pressure effects on thermodynamic properties of materials, we need a precise EOS. In previous study of SMM

theory [16], the authors derived EOS which describes the pressure versus volume relation of crystal lattice as

$$Pv = -r\left[\frac{1}{6}\frac{\partial U_0}{\partial r} + \frac{\theta X}{2k}\frac{\partial k}{\partial r}\right], \tag{15}$$

where P denotes the hydrostatic pressure, v is the atomic volume $v = V/N$ of a crystal having volume V and N atoms, and U_0 is the total potential energy of system.

By solving the above EOS we obtain the NND $r(P, T)$ between two intermediate atoms at pressure P and temperature T. Substituting the obtained $r(P, T)$ into Eqs. (2a), (2b), we find the quantities $k(P, T)$ and $\gamma(P, T)$. Using Eqs. (4), (12) and (14), respectively, we derive the values of the thermally induced lattice expansion $y_0(P, T)$, the atomic MSD $\langle u^2\rangle(P, T)$ and the parallel MSRD $\sigma^2(P, T)$ of cubic crystals at pressure P and temperature T as

$$y_0(P, T) = \sqrt{\frac{2\gamma(P, T)\theta^2}{3k^3(P, T)}A(P, T)}, \tag{16}$$

$$\langle u_i^2\rangle(P, T) = y_0^2(P, T) + \theta A_1(P, T) + \frac{\theta}{k(P, T)}(X - 1), \tag{17}$$

and

$$\sigma^2(P, T) \approx \frac{4\gamma^2(P, T)\theta^3}{k^5(P, T)}\left(1 + \frac{X}{2}\right)(X + 1) + \frac{2\theta X}{k(P, T)}, \tag{18}$$

where

$$A_1(P, T) = \frac{1}{k(P, T)}\left[1 + \frac{2\gamma^2(P, T)\theta^2}{k^4(P, T)}\left(1 + \frac{X}{2}\right)(X + 1)\right]. \tag{19}$$

The change of the crystal volume and Lindemann melting ratio $\xi(P, T)$ at pressure P and temperature T can be now determined, respectively, as

$$\frac{V}{V_0} = \frac{r^3(P, T)}{r^3(0, T)}, \tag{20}$$

and

$$\xi(P, T) = \frac{\sqrt{\langle u^2\rangle(P, T)}}{r(P, T)}. \tag{21}$$

3. Numerical calculations and discussion

For numerical calculations, the interatomic potential $\varphi(r)$ between two intermediate atoms of Kr crystal is assumed as Buckingham (exp-6) pair potential as follows

$$\varphi(r) = E_c\left\{\frac{6}{\alpha - 6}\exp\left[\alpha\left(1 - \frac{r}{r_0}\right)\right] - \frac{\alpha}{\alpha - 6}\left(\frac{r_0}{r}\right)^6\right\}, \tag{22}$$

where E_c is the cohesion energy, r_0 is the equilibrium nearest-neighbor distance, and α is parameter which is associated with the bulk modulus. For solid Kr crystal, the Buckingham potential parameters are, respectively, $E_c = 175.0\ k_B$, $r_0 = 4.12$ Å and $\alpha = 12.5$ [14]. Experimental measurement of melting temperature of solid Kr at ambient pressure is $T_{m0} = 115.79$ K.

In this work, the interaction energy of system is calculated by the coordination sphere method. The radius of the k-th coordination sphere is determined by $r_k = \nu_k a_0$, in which $a_0 = r_1$ is radius of the first coordination sphere. If we take into account the interaction of particles being on first five coordination spheres, the total potential energy U_0 of system has the form as

$$\begin{aligned} U_0 &= \tfrac{N}{2}\textstyle\sum_i \varphi_{i0}(|r_i + u_i|), \\ &= \tfrac{N}{2}E_c\left\{\tfrac{6}{\alpha-6}A_e\exp\left[\alpha\left(1 - \tfrac{a_0}{r_0}\right)\right] - \tfrac{\alpha}{\alpha-6}A_6\left(\tfrac{r_0}{a_0}\right)^6\right\}, \end{aligned} \tag{23}$$

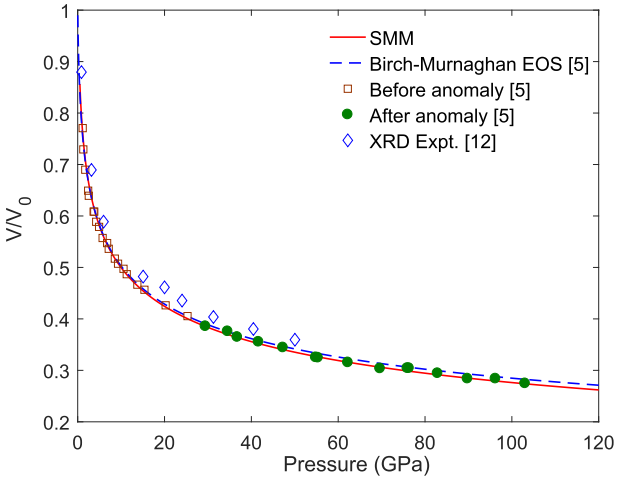

Fig. 1. Evolution of volume compressibility V/V_0 of solid Kr with pressure. Recent experimental measurements [5,12] and the fitted Birch-Murnaghan isothermal EOS [5] have been shown for comparison.

with the expressions of A_e and A_6 are respectively

$$\begin{aligned} A_e = z_1 + z_2\exp\left[\alpha(1 - \nu_2)\tfrac{a_0}{r_0}\right] + z_3\exp\left[\alpha(1 - \nu_3)\tfrac{a_0}{r_0}\right] + \\ z_4\exp\left[\alpha(1 - \nu_4)\tfrac{a_0}{r_0}\right] + z_5\exp\left[\alpha(1 - \nu_5)\tfrac{a_0}{r_0}\right], \end{aligned} \tag{24}$$

and

$$A_6 = z_1 + \frac{z_2}{\nu_2^6} + \frac{z_3}{\nu_3^6} + \frac{z_4}{\nu_4^6} + \frac{z_5}{\nu_5^6}, \tag{25}$$

where z_k is the number of particles being on the k-th coordination sphere with radius r_k. For the FCC lattice, we have $\nu_1 = 1$ and $z_1 = 12$, $\nu_2 = 1/\sqrt{2}$ and $z_2 = 6$, $\nu_3 = 1/\sqrt{3}$ and $z_3 = 24$, $\nu_4 = 1/2$ and $z_4 = 12$, $\nu_5 = 1/\sqrt{5}$ and $z_5 = 24$.

Before considering the pressure effects on EXAFS DWF and melting temperature of krypton, we firstly verify the precision of EOS derived in within the SMM scheme. Substituting total potential energy U_0 into Eq. (15) and solving this equation, we derive the values of NND $a(P, T)$, and then the change of volume V/V_0, at pressure P and temperature $T = 300$ K. In Fig. 1, the change of volume V/V_0 of krypton crystal with pressure at room temperature up to 120 GPa has been shown. Experimental data measured by high-resolution angle-dispersive synchrotron XRD by Errandonea et al. [12], *in situ* XRD and absorption by Rosa et al. [5] and the fitted Birch-Murnaghan isothermal EOS [5] have been shown for comparison. As it can be seen from this figure, the SMM EOS for solid Kr is in fair agreement with measurements to the highest experimental pressures, and consequently we can use the derived values of lattice constant for further investigation.

3.1. Pressure-dependent EXAFS Debye-Waller factor of krypton

In Fig. 2, we present the pressure effects (up to 50 GPa) on the atomic MSD of Kr crystal at temperature 300 K. The results of Monte-Carlo (MC) simulation based on empirical pair potentials [9] have also shown for comparison. The good agreement between our SMM calculations and MC simulation results could be observed. As we can see from this figure, the atomic MSD drops rapidly with the increasing of pressure, especially, below 5 GPa. From this result we can deduce that Kr crystal is relatively soft up to pressure 5 GPa and its volume will be changed rapidly under pressure range 0–5 GPa which can be verified by observing Fig. 1 above.

The pressure dependence (up to 50 GPa) of the MSRD or EXAFS Debye-Waller factor of Kr crystal at temperature 300 K has been displayed in Fig. 3. Our SMM calculations are consistent with previous results, especially, with values calculated by the MC simulations [9]

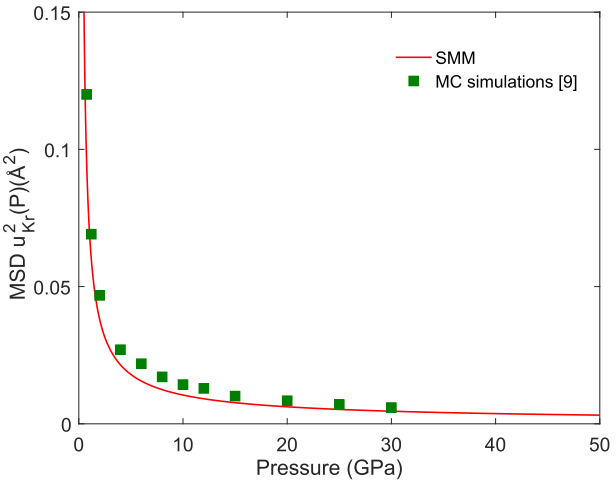

Fig. 2. High-pressure MSD of Kr. The Monte-Carlo simulations results [9] are shown for comparison.

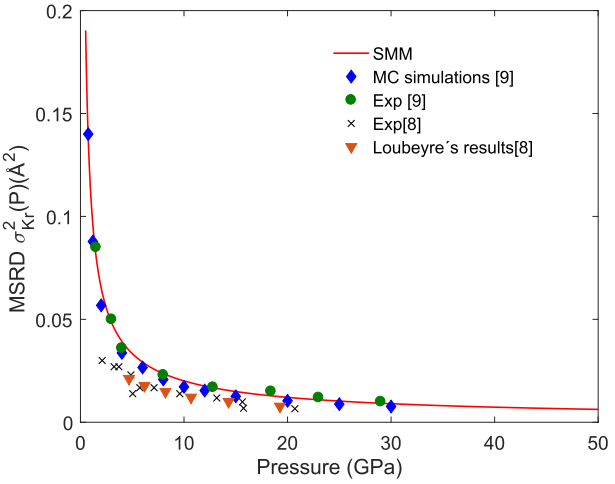

Fig. 3. High-pressure EXAFS DWF of Kr crystal. Other calculations and measurements [8,9] are shown for comparison.

and experimental measurements [9]. When the pressure increases, the MSRD of Kr crystal is going to decrease quickly. It is because of the limitation of atom fluctuation in crystal under high pressure. The reducing of EXAFS Debye-Waller factor predicts the decreasing of EXAFS signals when pressure increases. As we can see from Figs. 2 and 3, both quantities MSD and MSRD have identical reaction under pressure. They both drop rapidly with the increasing of pressure, especially, below 5 GPa.

3.2. High-pressure melting curve of krypton

In this subsection, the pressure effects on melting curve of Kr crystal is investigated by using the modified Lindemann criterion [21]. The Lindemann melting criterion was first proposed by Lindemann in 1910 that a material initiates melting process when the ratio $\xi = \sqrt{\langle u^2 \rangle}/r$ between square root of atomic mean-square vibration $\sqrt{\langle u^2 \rangle}$ and NND r reaches a threshold value ξ_0 [22]. Using the Lindemann criterion, the investigation of pressure-dependent melting temperature of materials has been performed by a lot of authors [23,24]. However, the authors showed that the classical Lindemann criterion is just useful for predicting melting points of crystalline materials under low pressure. When pressure increases (about pressure $P \geq 20$ GPa), results obtained from this model are not really good and are lower than those obtained from experimental measurements, theories and simulation calculations.

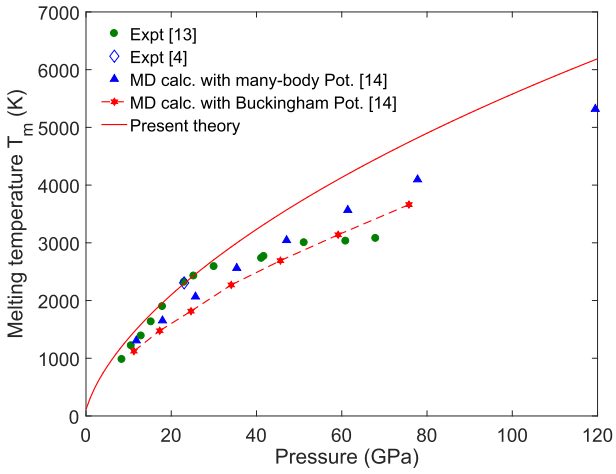

Fig. 4. The high-pressure melting curve of Kr crystal calculated by SMM (solid line). Closed circles represent the experimental data of Boehler et al. [13] and empty diamond represents melting measurement of Jephcoat and Besedin [4]. Pechenik et al.' calculations [14] using the many-body model (filled triangles) and the Buckingham potential (stars) have also shown for comparison.

In this paper, in order to calculate melting temperature of Kr crystal under pressure we use the modified Lindermann criterion which was applied effectively to evaluate the melting temperatures of a series of transition metals under high pressure [21]. The modified Lindermann criterion is based on the assumption that the ratio $\xi = \sqrt{\langle u^2 \rangle}/r$ remains constant for all range of studied pressure.

There are a number of published literatures concerning with the melting phenomenon of Kr crystal including experiments together with calculations. Its melting temperature was experimentally measured in a laser-heated DAC detected with the laser speckle method by Boehler et al. [13] up to pressure 61 GPa and by Jephcoat [4] at 23 GPa. On the theoretical side, the joint molecular dynamics (MD) simulations of the solid and the liquid phases sharing an interface, so-called the moving interface method, with the many-body potential and Buckingham pair potential were performed to investigate the melting curve of Kr up to pressure 120 GPa by Pechenik et al. [14].

In Fig. 4, the melting curve of Kr crystal calculated by SMM using Buckingham pair potential and compared to other theoretical and simulation calculations, and experimental measurements is shown. As it can be seen from this figure, our melting curve well reproduces the experimental measurements [4,13] up to the cusp reported by Boehler et al. [13]. Comparing to experiment of Boehler et al. [13], up to pressure 30 GPa, the error of melting temperature in SMM calculation is about 5%. At higher pressures, the appearance of discrepancy starts to be observed, with the calculated melting curve being increasingly higher than the experimental data. Our SMM calculations do not reproduce the cusp and the experimental melting points above it. Compared to the calculations by MD simulations of Pechenik et al. [14], our results are significantly higher than those of melting curves calculated with the many-body potential and Buckingham pair potential [14], especially, above pressure 20 GPa. The slope of melting predicted by corresponding method at 20 GPa is $dT/dP \sim 66$ K/GPa, while the average melting slope for the pressure range 20–120 GPa is $dT/dP \sim 41$ K/GPa.

In our opinion, the difference between present calculations and experimental measurements can be simply explained as: (i) the dependence of numerical results on empirical potential used. In present paper, the author assumed the interatomic interactions as the empirical Buckingham pair potential form which could not be strictly appropriate for the complex interactions in Kr crystal at high pressure. The embedded atom model based many-body potential should be more suitable for rare gases [14]. Nevertheless, Pechenik et al. [14] also proposed the

impossibility to reproduce both the EOS and the melting line with the same set of pair-potential parameters at high-enough pressures. (ii) the lack of paying attention to electron configurations of krypton. Experimentally, Boehler et al. [13] reported a considerable decrease in the melting slopes of Kr starting near 30 GPa, leading to the creation of cusp. According to Ross et al. [25], the steep lowering of the melting slope results from the formation of clusters in the liquid having icosahedral short-range order because of the hybridization of the 5*p*-like valence and 5*d*-like conduction states. As a consequence of it, in order to describe exactly high-pressure melting curve, the SMM approach needs to carefully pay attention to electronic properties of material.

4. Conclusions

In this work, the pressure effects on atomic mean-square displacement, EXAFS Debye-Waller factor and melting temperature of solid krypton have been investigated up to 120 GPa by means of the statistical moment method in statistical mechanics which has taken into account the anharmonicity effects of thermal lattice vibrations. Our numerical calculations are in good and reasonable agreements with available experimental data. Our work shows that the atomic mean-square displacement and EXAFS Debye-Waller factor of krypton crystal depend strongly on pressure, especially, at pressure below 5 GPa. About the pressure dependence of melting curve, our approach based on the modified Lindemann melting criterion can be suitable for evaluating the melting of Kr crystal up to 30 GPa. At higher pressure, SMM calculations do not reproduce the cusp and the experimental melting points above it. This approach gives us a relatively simple method for qualitatively calculating high-pressure thermo-physical properties of materials. Moreover, it can be used to verify future high-pressure experimental and theoretical works.

Acknowledgments

This research is funded by the Vietnam National Foundation for Science and Technology Development (NAFOSTED) under grant number 103.01-2017.343.

Appendix A. Supplementary data

Supplementary data to this article can be found online at https://doi.org/10.1016/j.cap.2018.11.005.

References

[1] S. Anzellini, A. Dewaele, M. Mezouar, P. Loubeyre, G. Morard, Science 340 (2013) 464 http://www.sciencemag.org/content/340/6131/464.full.pdf http://www.sciencemag.org/content/340/6131/464.abstract.
[2] Y. Fei, Science 340 (2013) 442 http://www.sciencemag.org/content/340/6131/442.full.pdf http://www.sciencemag.org/content/340/6131/442.short.
[3] Y. Ping, F. Coppari, D.G. Hicks, B. Yaakobi, D.E. Fratanduono, S. Hamel, J.H. Eggert, J.R. Rygg, R.F. Smith, D.C. Swift, et al., Phys. Rev. Lett. 111 (2013) 065501http://link.aps.org/doi/10.1103/PhysRevLett.111.065501.
[4] A.P. Jephcoat, Nature 393 (1998) 355 https://doi.org/10.1038/30712.
[5] A.D. Rosa, G. Garbarino, R. Briggs, V. Svitlyk, G. Morard, M.A. Bouhifd, J. Jacobs, T. Irifune, O. Mathon, S. Pascarelli, Phys. Rev. B 97 (2018) 094115https://link.aps.org/doi/10.1103/PhysRevB.97.094115.
[6] D. Young, Phase Diagram of the Elements, University of California Press, 1991.
[7] I. Kwon, L.A. Collins, J.D. Kress, N. Troullier, Phys. Rev. B 52 (1995) 15165 https://link.aps.org/doi/10.1103/PhysRevB.52.15165.
[8] A. Polian, J.P. Itie, E. Dartyge, A. Fontaine, G. Tourillon, Phys. Rev. B 39 (1989) 3369 https://link.aps.org/doi/10.1103/PhysRevB.39.3369.
[9] A. Di Cicco, A. Filipponi, J.P. Itié, A. Polian, Phys. Rev. B 54 (1996) 9086 https://link.aps.org/doi/10.1103/PhysRevB.54.9086.
[10] I. Aleksandrov, A. Zisman, S. Stishov, Sov. Phys. JETP 92 (1987) 371 http://www.jetp.ac.ru/cgi-bin/e/index/r/92/2/p657?a=list.
[11] A. Polian, J.M. Besson, M. Grimsditch, W.A. Grosshans, Phys. Rev. B 39 (1989) 1332 https://link.aps.org/doi/10.1103/PhysRevB.39.1332.
[12] D. Errandonea, B. Schwager, R. Boehler, M. Ross, Phys. Rev. B 65 (2002) 214110https://link.aps.org/doi/10.1103/PhysRevB.65.214110.
[13] R. Boehler, M. Ross, P. Söderlind, D.B. Boercker, Phys. Rev. Lett. 86 (2001) 5731 https://link.aps.org/doi/10.1103/PhysRevLett.86.5731.
[14] E. Pechenik, I. Kelson, G. Makov, Phys. Rev. B 78 (2008) 134109https://link.aps.org/doi/10.1103/PhysRevB.78.134109.
[15] N. Tang, V.V. Hung, Phys. Status Solidi (b) 149 (1988) 511 ISSN 1521-3951, https://doi.org/10.1002/pssb.2221490212.
[16] N. Tang, V.V. Hung, Phys. Status Solidi (b) 162 (1990) 371 ISSN 1521-3951, https://doi.org/10.1002/pssb.2221620206.
[17] V.V. Hung, J. Lee, K. Masuda-Jindo, P.T.T. Hong, J. Phys. Soc. Jpn. 75 (2006) 024601.
[18] K. Masuda-Jindo, V.V. Hung, P.D. Tam, Phys. Rev. B 67 (2003) 094301http://link.aps.org/doi/10.1103/PhysRevB.67.094301.
[19] E.D. Crozier, J.J. Rehr, R. Ingalls, D.C. Koningsberger, R. Prins, X-Ray Absorption: Principles, Applications, Techniques of EXAFS, SEXAFS and XANES, first ed., Wiley-Interscience, 1988ISBN 0471875473 http://www.amazon.com/X-Ray-Absorption-Principles-Applications-Techniques/dp/0471875473.
[20] G. Bunker, Nucl. Instrum. Methods Phys. Res. 207 (1983) 437 ISSN 0167-5087, http://www.sciencedirect.com/science/article/pii/0167508783906555.
[21] H.K. Hieu, J. Appl. Phys. 116 (2014) 163505http://scitation.aip.org/content/aip/journal/jap/116/16/10.1063/1.4899511.
[22] F. Lindemann, Phys. Z. 11 (1910) 609.
[23] D. Errandonea, Phys. B Condens. Matter 357 (2005) 356 ISSN 0921-4526 http://www.sciencedirect.com/science/article/pii/S0921452604012396.
[24] H.K. Hieu, N.N. Ha, AIP Adv. 3 (2013) 112125http://scitation.aip.org/content/aip/journal/adva/3/11/10.1063/1.4834437.
[25] M. Ross, R. Boehler, P. Söderlind, Phys. Rev. Lett. 95 (2005) 257801https://link.aps.org/doi/10.1103/PhysRevLett.95.257801.